Chemical Physics Letters 456 (2008) 110–115

Contents lists available at ScienceDirect

Chemical Physics Letters

journal homepage: www.elsevier.com/locate/cplett

Nickel doped spinel lithium manganate – some insights using opto-impedance

K. Ragavendran [a], A. Nakkiran [b], P. Kalyani [c], A. Veluchamy [a], R. Jagannathan [a,*]

[a] *Central Electrochemical Research Institute, Karaikudi 630 006 (TN), India*
[b] *Center for Education, CECRI, Karaikudi 630 006, India*
[c] *Department of Chemistry, Thiagarajar College of Engineering, Madurai 625 015, India*

A R T I C L E I N F O

Article history:
Received 18 October 2007
In final form 5 March 2008
Available online 10 March 2008

A B S T R A C T

Opto-impedance studies on spinel type pristine and Ni-doped $LiMn_2O_4$, an important cathode system for Li-ion batteries have revealed the difference in electronic structure arising out of the Ni-substitution. The opto-impedance spectra of Ni-doped $LiMn_2O_4$ even under dark condition exhibits a more complex structure(two semicircles with some skewed structure) suggesting the presence of defect structure(s) remaining dormant which upon UV shining get merged to form a single semicircle. Qualitatively this aliovalent substitution modifies the charge transfer state and activates a defect initiated Warburg diffusion process with a time scale of $\sim 50\ \mu s$.

1. Introduction

Doped transition metal oxides in general, manganites and manganates in particular, constitute an important branch of research for condensed matter physicists and material researchers. Of special importance is the spinel type lithium manganate showing potential for application as cathodes for high energy density Li-batteries [1] apart from being a frustrated antiferromagnetic lattice system [2], possessing interesting magnetic properties [3] and finding applications as a prototype material in the study of charge ordering in strongly correlated electron systems [4]. Doping at the manganese site of these oxides is an interesting topic of study. Among the dopants, Ni is one of the most fascinating members. Nickel doping at the Mn site of perovskite manganites has been studied to understand the origin of low-field magneto resistance [5]. Ni doping at the Mn site of spinel manganates is reported to enhance its electrochemical performance in terms of higher cell voltage, improved cyclability, capacity, and so on [6]. However, the exact mechanism explaining the role of a dopant ion leading to such an enhancement in performance seems to be not well established. Also, nickel doped lithium manganate shows unique cyclic voltammetric responses compared to pristine and other transition metal doped lithium manganates [7] which is not yet well understood.

Motivated by the success of using opto-impedance as a probe to study electronic phenomena in oxides such as quantum blinking in $Y_2O_2S{:}Eu^{2+}$ nanostructures [8] and trap states in $LiMn_2O_4$ and $Nd_{0.7}Sr_{0.3}MnO_3$ [9,10], we extend the technique as an attempt to understand the effects of Ni doping in lithium manganate.

2. Experimental aspects

The experimental procedures employed for the sample(s) synthesis through fuel assisted combustion route, characterization and opto-impedance measurements were the same as described before [9,10]. Special care was employed in the sample synthesis to ensure the absence of Ni-contamination in the pristine sample. Solid state AC impedance studies (under dark and UV shined conditions) on polycrystalline $LiMn_2O_4$ and $LiNi_{0.1}Mn_{1.9}O_4$ were measured using EIS Princeton Applied Research – AC impedance analyzer in the frequency range 100 kHz to 10 Hz with an AC amplitude of 20 mV. The frequency range employed in the study is too small to detect any intra-grain effect and hence the signal we observe is probably only due to the electronic changes at the grain boundary interface. It is also pertinent to note that all our experiments were carried out at room temperature (300 K) which is very close to the charge ordering transition temperature of lithium manganate, i.e. 280 K [4].

3. Results and discussion

3.1. Ni-doping in spinel $LiMn_2O_4$

Pristine $LiMn_2O_4$ adopts a cubic *Fd*3*m* space group which upon Ni-doping reduces the lattice symmetry to a tetragonal $P4_332$ space group [11]. Correspondingly, the Wyckoff position for the sites occupied by the transition metal ion(s) ($Mn^{3+/4+}$ and $Ni^{4+/2+}$) changes from octahedral 16(d) to octahedral 4(b) and 12(d), respectively. From the structural data we have that in the Ni-doped spinel system, Li ions occupy an 8a site while the transition metal ions (Mn/Ni) are in 16d sites This may lead to a change in the d-orbital energy levels of these ions that would eventually bring

---

[*] Corresponding author.
E-mail address: jags57_99@yahoo.com (R. Jagannathan).

0009-2614/$ - see front matter © 2008 Elsevier B.V. All rights reserved.
doi:10.1016/j.cplett.2008.03.016

out some difference in the d-orbital splitting. In this system, the Mn-ion can exist both in 3+($3d^4$) and in 4+($3d^3$) states while Ni occupying the Mn-site can have both 2+($3d^8$) and 4+($3d^6$) states and hence come under aliovalent doping. The charge transfer energy of d^6 ion(s) in the case of nickel will be shifted to a higher energy for the reason that the lower t_{2g} orbital is completely filled [12]. Using first-principles methods, Shi et al. [13] have explained that in Ni-doped lithium manganate the density of states of oxygen 2p orbitals will shift to a lower energy eventually raising the cell voltage to higher values. This means that in the Nernst equation, the redox potential of the transition metal ion(s) raises to a higher energy that would in turn raise the cell voltage. The substitution of more electronegative Ni (electronegativity $\chi_{\mathrm{Ni}} = 1.9$) for manganese ($\chi_{\mathrm{Mn}} = 1.5$) will lead to more covalent bonding with the surrounding oxygens which in turn might ask for more binding energy. Also, using ultraviolet photo-electron spectroscopy (UPS) Gao et al. [14] have explained the higher cell voltage in Li-batteries using Ni-substituted spinel cathodes, on the basis of higher binding energy for Ni 3d electrons. These arguments relate to the average matrix potential of the system.

For the opto-impedance results on the Ni-doped spinel, on the other hand, we should consider defects generated and their relaxation kinetics.

The substitution of Ni^{2+} in $\mathrm{Mn}^{4+/3+}$ site can be considered as a n-type substitution because it carries a negative effective charge given by (following Kroger-Vink notations)

$$x\mathrm{Ni}_2^{2+/4+}\mathrm{O}_3 + \mathrm{LiMn}_{2-x}\mathrm{O}_4 \xrightarrow{\Delta(\mathrm{O}_2)} \mathrm{LiMn}_{2-x}\,\mathrm{Ni}^{2+''}_{\mathbf{Mn}^{3+/4+}} + 2\hat{\mathrm{h}} \tag{1}$$

Hence, this may generate electronic defects (comprising a complex defect center in the vicinity of $\mathrm{Ni}_{\mathrm{Mn}}$ site) near the conduction band in the vicinity of the fundamental band-edge region (~4 eV). These itinerant defects or electron–holes created can relax or may get activated when energized suitably either electrically or optically to the extent of 4 eV. In spite of the importance of the knowledge on the different types of defects, there has been little information about the defects in $\mathrm{LiMn_2O_4}$ because of the difficulty to observe them directly through experiments [15]. It is pertinent to note that recently Wakihara et al. [16] have demonstrated using first principles calculations the importance of defect structure in determining the cathode performance of $\mathrm{LiMn_2O_4}$ in Li-batteries.

3.2. Opto-impedance spectra

Opto-impedance spectra (Complex plane impedance plots under dark and UV shined conditions) are given in Figs. 1 and 2 for $\mathrm{LiMn_2O_4}$ and $\mathrm{LiNi_{0.1}Mn_{1.9}O_4}$ samples, respectively. In these plots, goodness of fit (R^2) could be improved when they were split into several components. Hence, these profiles can be fitted either as a simple or composite of several linear/non-linear parts under second order equation(s) or as a simple loop when fitted using a fourth order polynomial. But for practical reasons we limited our fit to a second-order quadratic equation with the experimental constants determined by the condition of the cathode sample(s).

Fig. 3a and b represent the RC fit to the complex plane impedance pattern of $\mathrm{LiMn_2O_4}$ under dark and UV shined conditions, respectively. Fig. 4a and b represent the RC fit to the complex plane impedance pattern of $\mathrm{LiNi_{0.1}Mn_{1.9}O_4}$ under dark and UV shined conditions, respectively. The fitted data are given in Table 1. From Figs. 1 and 2, one can observe that the center of the arcs is displaced below the real axis because of the presence of the distributed elements in the system (a characteristic property of the disordered materials). Due to this fact, the relaxation time τ is not single valued but is distributed either continuously or discretely around a mean, $\tau_{\mathrm{m}} = \omega_{\mathrm{m}}{}^{-1}$. It is interesting to note that the dispersion angle for the compound $\mathrm{LiNi_{0.1}Mn_{1.9}O_4}$ is lower when compared to that of $\mathrm{LiMn_2O_4}$.

The following generalizations have become possible: The complex plane impedance plots for the pure spinel $\mathrm{LiMn_2O_4}$ show simple semicircular patterns, both under dark and under UV shined conditions with a moderate decrease in impedance (~15%) under UV irradiation, which can be attributed to photo-generated carriers. The semicircular impedance pattern can be explained by considering a capacitor element in parallel with a bulk resistance due to the dielectric $\mathrm{LiMn_2O_4}$ constituting a parallel RC network.

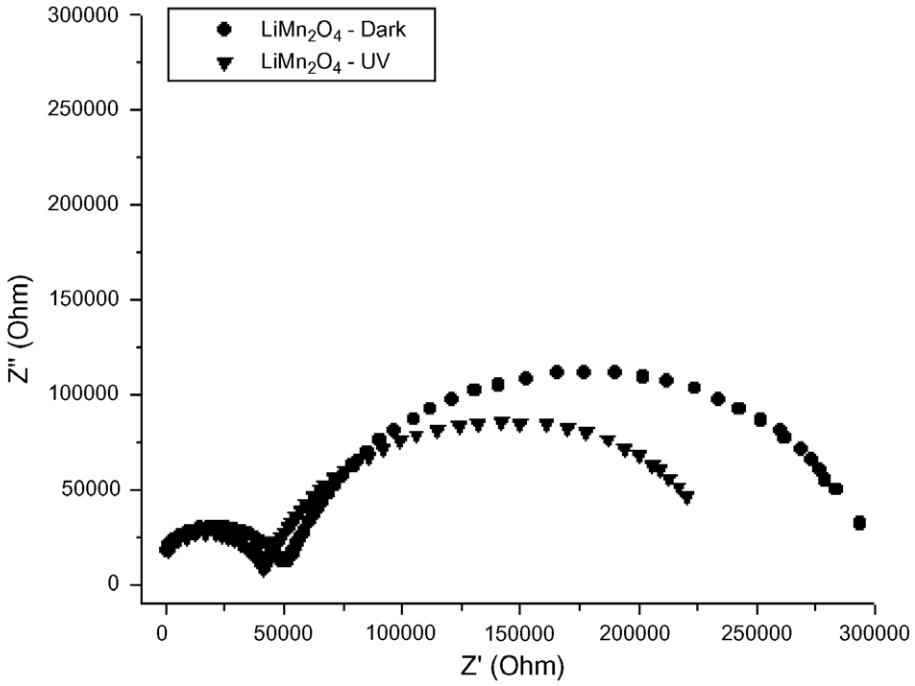

Fig. 1. Opto-impedance pattern of $\mathrm{LiMn_2O_4}$.

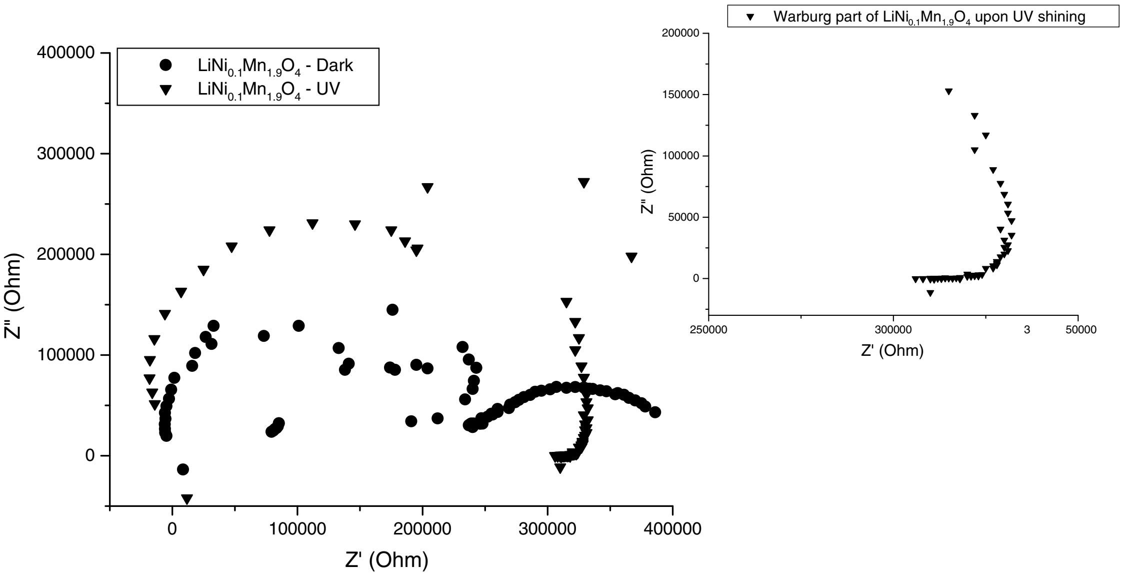

Fig. 2. Opto-impedance pattern of $LiNi_{0.1}Mn_{1.9}O_4$. Inset: Expanded impedance profile signifying a Warburg type diffusion process in the low frequency region.

Turning to the Ni-substituted system, the picture is more complex in that UV irradiation generates additional processes apart from semi-circular patterns. For this system, both dark and UV shined conditions show many fascinating results (Fig. 2). Under dark condition, we can see the appearance of two semicircles, with the first semicircle appearing in the high frequency side showing some structure with inward skewing. This may be due to vacancy related defect structures activated even under dark conditions. Also we can notice that the curvature of the second semicircle (semicircle-II) occurring in the low frequency region is not very pronounced. Upon UV shining, the two semicircles merge to form a single circle with the center shifting towards mid-frequency region.

It is evident from the impedance data that the semicircle in the high frequency region (12–40 kHz) does not undergo substantial change with the transition metal doping while the other one in the low frequency 50–60 Hz (marked 'semicircle 2') does undergo significant change with the transition metal doping both under dark and UV perturbations. Especially, the curvature of the second semicircle is not very pronounced as does the semicircle 1, instead this appears as a flat-linear region. These observations suggest that the former can be assigned to Li-related centers while the latter to transition metal ($Mn^{3+-4+}/Ni^{2+/4+}$) related centers.

In the spinel system, there are two types of centers present: (a) Li vacancy/$Li^+ \leftrightarrow$ Li intercalation related centers and (b) the redox couple centering around the transition metal species involved in the electron transfer processes. The former process involving the vacancies of both types (anionic, cationic) can be analogized to F-type colour centers because electron transfer involved during the intercalation process will trap the electrons at the anion vacancies. Also, the aliovalence between Mn and Ni redox couples in $LiNi_{0.1}Mn_{1.9}O_4$ will create charge compensating defects. It is thus reasonable to expect these two types of electron centers getting localized in the vicinity of the respective species. This manifests as shown in Fig. 4a as a gap between the two semicircles, and the two semicircles tend to avoid each other in the dark condition which is turned inside out to yield practically a single semicircle in the UV shined condition (Fig. 4b), facilitating a charge buildup. This, along with the respective bulk resistances can contribute to two parallel resistor–capacitor combination thereby accounting for the presence of two semi-circular impedance profiles for the Ni-doped spinel under dark condition.

Furthermore for the Ni-substituted sample, a step-like linear portion in the low frequency region around 10–50 Hz emerges while such a feature does not occur for the pristine sample. Hence it looks possible that the charge distribution in $LiNi_{0.1}Mn_{1.9}O_4$ under the dark condition gets activated upon UV-shining to follow a streamlined process such as a diffusion or spatially localized distribution of charges.

Changes in the impedance parameters between dark and UV-shined conditions for pure and Ni-doped lithium manganate are compared in Table 2. From the table, we observe that both the pristine and the Ni-doped lithium manganate exhibit a capacitive effect. It is pertinent to mention here that the contributions from electrical contacts with the capacitance value of $\sim 1 \times 10^{-14}$ F compared to value of the 1×10^{-11} F being three orders lower can be ignored for all practical considerations. While UV irradiation causes only a moderate change in the real part of the impedance value ($\pm\Delta R \sim 50\%$) which can be explained in terms of trap states that either quench or facilitate photo-conductivity, and also in terms of optical bleaching of color centers. The phenomenal four-fold decrease ($\Delta Z_c \sim 400\%$) in capacitive impedance (imaginary part of impedance along the y-axis) for semicircle 2 of the pure and the unique semicircle of the Ni-doped samples under optical pumping makes an interesting observation.

The proportional increase in capacitance upon UV perturbation might stem from the modified charge density distribution with the centers of gravity of positive and negative charges shifting closer through a charge transfer absorption centering around the transition metal species. In other words, the capacitive effect and hence the sensitivity to external perturbations (AC-frequency and UV irradiation) observed in these spinel type manganese oxides (at the near vicinity to the charge ordering transition temperature) may have some close analogy with the drastic spin clusters exhibited by perovskite manganese oxides around T_c [17].

It can also be seen from Fig. 2 that UV shining on Ni-doped spinel generates a Warburg component with the parameters being $W_sR = 3.263 \times 10^8\ \Omega$; $W_sT = 5.39 \times 10^{-5}$ s. In impedance spectroscopy, a linear portion having a slope, $\tan 45^\circ \sim 1$, will correspond to a Warburg impedance representing a diffusion dominated process. Warburg impedance attributed to the diffusion of charged species can be given by

$$W_sR = R_W \tanh \sqrt{j\omega T_W}/\sqrt{j\omega W_s T} \quad (2)$$

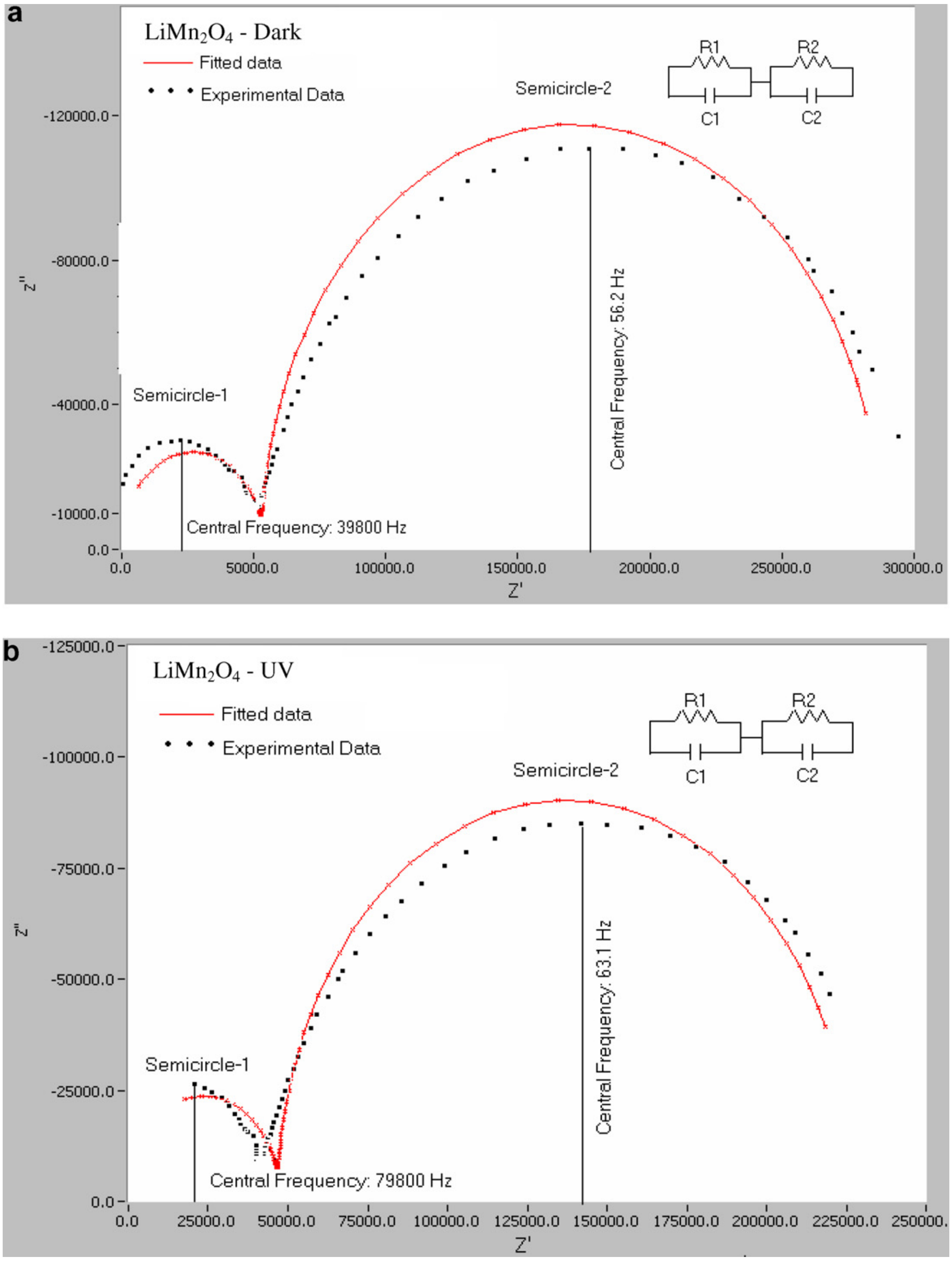

Fig. 3. (a) AC-impedance pattern (Nyquist plot) of $LiMn_2O_4$ under dark condition fitted with a two RC parallel circuit model and (b) AC-impedance pattern of $LiMn_2O_4$ (Nyquist plot) under UV shined condition fitted with a two RC parallel circuit model.

With R_W and T_w being Warburg resistance and time constant, respectively. It can be seen that UV shining on Ni-doped spinel generates a Warburg component with the parameters being $W_sR = 3.263 \times 10^8\ \Omega$; $W_sT = 5.39 \times 10^{-5}$ s. This means that upon UV shining in the low frequency region of the impressed voltage, a kinetic process sets in with a time-constant value of about 50 μs.

Dahn et al. [18,19] have used a lattice-gas model for explaining the enhancement in electrochemical capacity and the cell voltage of lithium manganate based cells. On the basis of the lattice gas model, the two plateaus observed in the voltage-profile at 4.1 and 4.7 V can be attributed to the ordering of Li-atoms at $y = 1/2$ onto only one of the two inter-penetrating face centered cubic (fcc) lattices. On the otherhand, Ni-ions replacing Mn-site is distributed over the 16d sites of Mn-ions randomly distributed over the entire two sub-lattices. The emergence of a single semicircular pattern in the case of $LiNi_{0.1}Mn_{1.9}O_4$ upon UV shining enables us to hypothesize that the identities for the two kinds of cationic sites in the spinel may no longer exist due to the combined influence of the modified charge transfer process and Warburg diffusion occurring in the above compound upon UV shining.

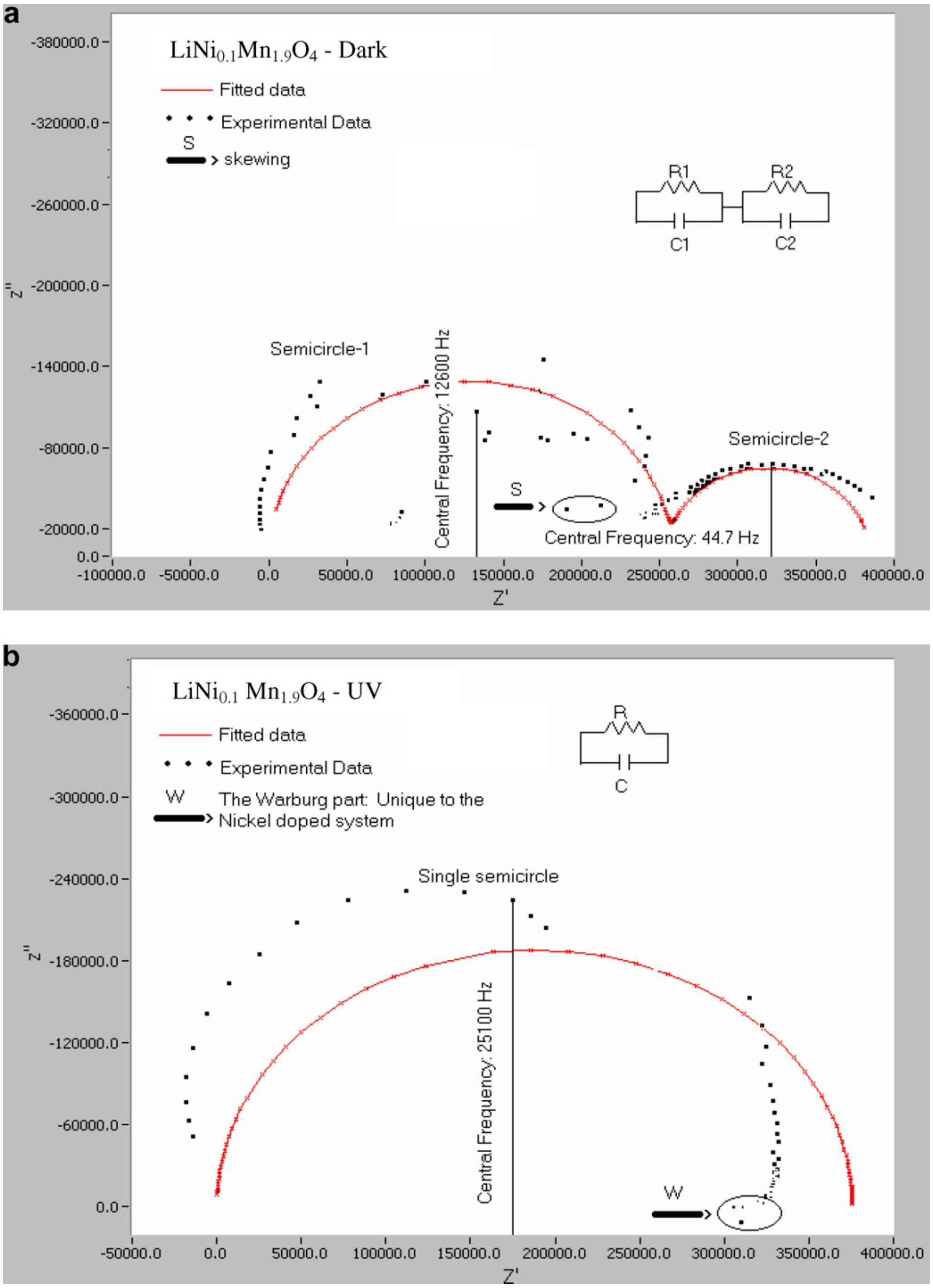

Fig. 4. (a) AC-impedance pattern of $LiNi_{0.1}Mn_{1.9}O_4$ (Nyquist plot) under dark condition fitted with a two RC parallel circuit model and (b) AC-impedance pattern of $LiNi_{0.1}Mn_{1.9}O_4$ (Nyquist plot) under UV shined condition fitted with a single RC parallel circuit model.

Table 1
Fitted impedance parameters for pristine and nickel doped lithium manganate (estimated parameters errors: $\delta = 3\%$)

System	Condition	Impedance parameters (fitted)							
		First semi-circle				Second semi-circle			
		R_1 (Ω)	C_1 (Farad)	Central freq. (Hz)	Comments	R_2 (Ω)	C_2 (Farad)	Central freq. (Hz)	Comments
$LiMn_2O_4$	Dark	53034.98	9.2074E−11	39800	–	234983.58	1.12E−8	56.2	–
	UV	22027	1.0612E−10	79400	–	60261.3	5.81E−8	63.1	–
$LiNi_yMn_{2-y}O_4$	Dark	256452	5.0358E−11	12600	–	127832	2.13E−8	44.7	–
	UV	374810	2.3905E−10	25100	–	–	–	–	On set of a Warburg type diffusion[a]

[a] Warburg diffusion parameters: W_sR: 3.263e^8 Ω and W_sT: 5.39e^{-5} s.

Table 2
Change in impedance parameters between dark and UV shined conditions for pure and nickel doped lithium manganate

System	First semi-circle (%)	Second semi-circle (%)
$LiMn_2O_4$	$-\Delta R = 58.46$ $+\Delta C = 15.25$	$-\Delta R = 74.35$ $+\Delta C = 418.75$
$LiNi_yMn_{2-y}O_4$	$+\Delta R = 46.15$ $+\Delta C = 374.7$	

ΔR and ΔC, respectively indicate the change in resistance and capacitance value of the sample after UV irradiation. The positive sign indicates an increase in the parameter value upon UV irradiation.

4. Conclusions

Perovskite CMR manganites and spinel type lithium manganates bear several similarities. Both possess interesting magnetic properties and have a manganese octahedra with the Mn^{3+}/Mn^{4+} redox couple. The ratio of 3+ and 4+ state of Mn and their competing interactions with the oxygen backbone determine the physical properties and their response to optical perturbation. Extensive literature on $LiMn_2O_4$ and its doped varieties as a cathode material for lithium batteries is available. However, the literature on the physics of this compound seems to be scarce. In the present Letter we have reported for the first time the sensitivity of nickel doped lithium manganate to external perturbation (UV shined AC-impedance). Ni doping replaces some Mn^{3+} and modifies the charge transfer process in the Mn^{3+}–O–Mn^{4+} redox complex. Furthermore, the divalent Ni in the trivalent Mn site being aliovalent doping generates defect centers relaxing through a Warburg type diffusion process, upon optical pumping, with a time-constant value of $\sim$50 μs. These arguments may be useful to have a better understanding on the unexplained phenomena of a one-step discharge curve in Nickel doped spinels in contrast with the two-step discharge curve in pristine lithium manganate [7]. Finally, we should note that a final description of the defect states and whether the charge transfer state is weak bond [20] and or spin [21] related is still a distance away.

Acknowledgments

One of the authors (K.R) wishes to thank the CSIR, New Delhi (Govt. of India), for the award of a senior research fellowship. Our sincere thanks to the Department of Science and Technology, New Delhi, for the Grant # 100/(IFD)/17/2007-08 received for this work. It is a pleasure to thankfully acknowledge the critical comments and valuable suggestions from the referee(s).

References

[1] M. Stanley Whittingham, Chem. Rev. 104 (2004) 4271.
[2] K. Yamaura et al., J. Am. Chem. Soc. 128 (2006) 9448.
[3] R. Basu, C. Felser, A. Maignan, Ram Seshadri, J. Mater. Chem. 10 (2000) 1921.
[4] J. Rodriguez Carvajal, G. Rousse, C. Masquelies, M. Hervieu, Phys. Rev. Lett. 81 (1998) 4660.
[5] S. Pal, E. Bose, B.K. Chaudhuri, H.D. Yang, S. Neeleshwar, Y.Y. Chen, J. Magn. Magn. Mater. 293 (2005) 872.
[6] H. Amine, H. Tukamoto, H. Yasuda, H. Fujita, J. Electrochem. Soc. 143 (1996) 1607.
[7] T. Ohzuku, S. Takeda, M. Iwanaga, J. Power Sources 81–82 (1999) 90.
[8] A. Nakkiran, J. Thirumalai, R. Jagannathan, Chem. Phys. Lett. 436 (2007) 155.
[9] P. Kalyani et al., J. Phys. D: Appl. Phys. 38 (2005) 990.
[10] K. Ragavendran, V. Morchshakov, A. Veluchamy, Klaus Bärner, J. Phys. Chem. Solids 69 (2008) 182.
[11] P. Strobel, A. Ibarra-Palos, M. Anne, C. Poin Signon, A. Crisci, Solid State Sci. 5 (2003) 1009.
[12] Y.J. Wei, L.Y. Yan, C.Z. Wang, X.G. Xu, F. Wu, G. Chen, J. Phys. Chem. B 1088 (2004) 18547.
[13] S. Shi, C. Ouyang, D. Shen Wang, L. Chen, X. Huang, Solid State Commun. 126 (2003) 531.
[14] Y. Gao, K. Myrtle, M. Zhang, J.N. Reimers, J.R. Dahn, Phys. Rev. B 54 (1996) 16670.
[15] T. Minami, M. Tatsumisago, M. Wakihara, C. Iwakura, S. Kohjiya, I. Tanaka, Solid State Ionics for Batteries, Springer, Tokyo, 2005. p. 259.
[16] Y. Koyama, I. Tanaka, H. Adachi, Y. Uchimoto, M. Wakihara, J. Electrochem. Soc. 150 (2003) A63.
[17] J.M. De Teresa et al., Nature 386 (1997) 256.
[18] T. Zheng, J.R. Dahn, Phys. Rev. B 56 (1997) 3800.
[19] Y. Gao, J.N. Reimers, J.R. Dahn, Phys. Rev. B 54 (1996) 3878.
[20] D.L. Staebler, C.R. Wronski, Appl. Phys. Lett. 31 (1977) 292.
[21] New Trends in the Characterization of CMR manganites and Related Materials. Ed. K. Bärner, Published by Research sign post 2005, ISBN: 81-308-0043-8, p. 278.